



Investigation on the Agent Precise Quantitative Control for Foam Technology with Cavitation Jet

X. Lu^{1,2,3†}, Y. Han¹, C. Shen¹, Y. Xing¹ and G. Shi¹

¹ School of Emergency Management and Safety Engineering, China University of Mining and Technology (Beijing), Beijing 100083, PR China

² State Key Laboratory Cultivation Base for Gas Geology and Gas Control, Henan Polytechnic University, Jiaozuo 454150, PR China

³ State Key Laboratory of Coal Resources and Safe Mining, China University of Mining and Technology (Beijing), Beijing 100083, PR China

†Corresponding Author Email: luxinxiao123@163.com

(Received June 30, 2020; accepted December 2, 2020)

ABSTRACT

A reliable agent addition control is crucial for the foam technology that is prevalent in many industrial fields. The objective of this paper is to reveal the precise quantitative control mechanism and distinctive performance of cavitation jet. The cavitation evolution suction process is analyzed by the vapor appearance order defined. A 5-6 mm vapor-liquid transition interface is found in the cavitation jet with a remarkable mutation in fluid pressure, density and velocity. The vapor region in the jet device decreases and the maximum vapor volume fraction declines from 96.4% to 0 as the pressure ratio increases. The precise quantitative control is realized by the cavitation jet at the negative pressure less than -87 kPa in the suction port. The absorption amount decreases with the absorbed liquid viscosity increasing and a various level of precise quantitative control is achieved by the orifice plate area. The relation between the absorption amount and plate area is quadratic curve. Furthermore, the dust suppression practical was successfully conducted in a coal bunker to verify the effectiveness of foam technology using cavitation jet. Based on the above contribution, it is believed that the proposed precise quantitative control method has a strong applicability and popularization in industrial control field.

Keywords: Jet cavitation; Flow control; Vapor; Pressure ratio; Dust control.

1. INTRODUCTION

Foam technology is prevalent in many industrial fields, such as fire extinguishment, oil refining, chemical industries, dust suppression, and nuclear engineering, *et al* (Aloui and Madani 2007; Hernandez-Alvarado *et al.* 2018; Xi *et al.* 2019; Wang 2015). As shown in Fig. 1, the foaming system is the core for foam technology, which in general consists of two primary units that are agent addition component and foam maker component. As a key component of foam technology, the agent addition affects the reliable operation of foaming system. For instance, related literature has shown that the unreliable agent addition restricted the popularization of foam technology in dust suppression field subjected to its complex operation or inflexible equipment (Wang *et al.* 2012).

To realize a convenient operation of agent addition, the high-velocity hydraulic jet is in universal use due

to its advantage of small volume, no moving parts, simple structure, low maintenance, simple compact and easy to install (Lu *et al.* 2014; Shah *et al.* 2011). The working principle of hydraulic jet is to generate a negative pressure and then to absorb liquid (Jia *et al.* 1993). However, a great fluctuation of agent suction may be caused by a slight change in the working condition since the negative pressure and absorption process are sensitive to the outlet pressure of jet device (Cunningham *et al.* 1970; Zhu *et al.* 2017). As for an unsteady thermodynamic system, foam produces an inevitable pressure fluctuation that is bound to influence the agent addition performance of hydraulic jet. Therefore, it is necessary to investigate a new reliable hydraulic jet to achieve a stable agent addition.

In this paper, a method of liquid suction based on the jet cavitation principle is proposed to deal with the bottleneck problem of addition instability. Masses of relevant literatures have shown that this method is

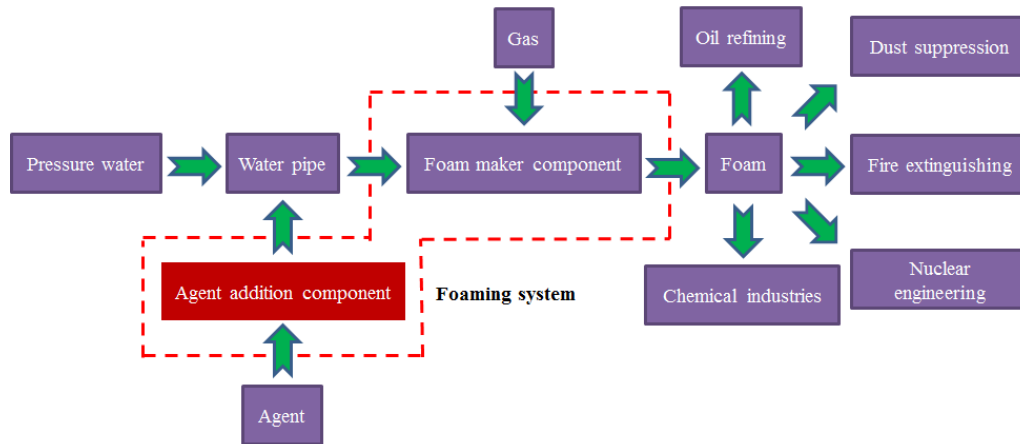


Fig. 1. Agent addition component of foaming system.

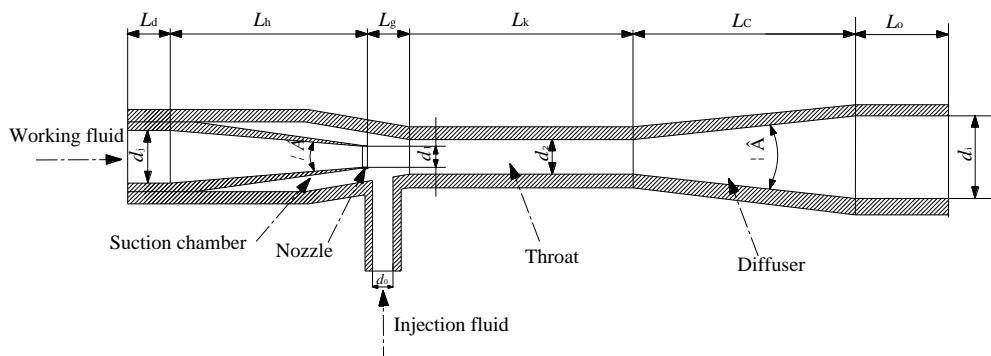


Fig. 2. Schematic diagram of jet device.

theoretically feasible. Harvey (1970), and Huzel and Huang (1992) indicated that the venturi used in the rocket propulsion system can control the fuel flow accurately at the cavitation operation. The propellant mass flow rate maintains at a constant when the pressure ratio reduces to a critical value even the downstream pressure changes rapidly due to the start-up transient or combustion oscillation (Abedini *et al.* 2014; Zhu *et al.* 2018). Meanwhile, related research (Ghassemi and Fasih, 2011; Ulas 2005) raised to use the hydraulic jet to induce cavitation and then control flow. This achievement is employed to design a high precision flowmeter, throttle valve and control unit that has obtained remarkable benefits. However, the previous research only involved the mainstream control at the cavitation condition without liquid addition. On the basis of hydraulic cavitation jet theory, researchers explore to perform a trial on the agent addition at the cavitation condition. Zhu *et al.* (2017) designed a cavitation venturi device to improve accuracy and stability of mini quantitative liquid adding with the cavity cloud, axial pressure distribution and pressure ratio discussion. Through optimize the jet structure, the operating range for the cavitating quantitative mixing devices is extended (Zhu *et al.* 2018). While, there is no mechanism revelation on achieving the quantitative absorption that is important for further research on the cavitation jet.

The objective of the present paper is to reveal the precise quantitative control mechanism and distinctive performance of cavitation jet. The research focuses on the vapor evolution law and quantitative suction characteristics under the cavitation operation condition. The intrinsic relevance between the stable suction process and cavitation interface is illuminated systematically. The precise suction features are investigated under different pressure ratio and absorbed liquid viscosity. Furthermore, a various level of precise quantitative control is evaluated at different orifice plate area. With the realization of agent precise quantitative control, field trials of foam technology for dust suppression were carried out at a coal bunker to verify the practical effectiveness of cavitation jet.

2. FUNDAMENTAL EQUATION AND GEOMETRIC MODEL OF JET CAVITATION

2.1 Fundamental Equation

Figure 2 exhibits the jet device that is mainly composed of nozzle, suction chamber, throat, suction port and diffuser. Jet device uses turbulence flow to form negative pressure in the suction chamber and drives the absorbed liquid into device, along with a

mass, energy and momentum exchange between the working fluid and absorbed fluid (Dong 2005).

Cavitation suction process of jet device involves phase state conversion of multi-phase flow that is unsteady and incompressible flow. The fluid velocity inside the jet device is relatively high, which is mostly turbulent jet. Since the realizable $k-\varepsilon$ model satisfies mathematical constrains of Reynolds stresses, it is conforms to the physical properties of turbulence. The $k-\varepsilon$ model is chosen because it has good performance for flows with complex secondary flow characteristics and boundary layer flows under strong adverse pressure gradients, separation and recirculation (Morgut *et al.* 2011; Shih *et al.* 1995; Tseng and Wang 2014). The equation of continuity, momentum, energy, k and ε is expressed as:

$$\frac{\partial \rho}{\partial t} + \frac{\partial \rho u_i}{\partial x_i} = 0 \quad (1)$$

$$\frac{\partial \rho u_i}{\partial t} + \frac{\partial}{\partial x_i} (\rho u_i) = -\frac{\partial P}{\partial x_i} +$$

$$\frac{\partial}{\partial x_j} \left[(u + u_t) \left(\frac{\partial u_i}{\partial x_j} + \frac{\partial u_j}{\partial x_i} \right) \right] \quad (2)$$

$$\frac{\partial (\rho k)}{\partial t} + \frac{\partial (\rho u_i k)}{\partial x_i} = \frac{\partial}{\partial x_j} \left[\left(\mu + \frac{\mu_t}{\sigma_k} \right) \frac{\partial k}{\partial x_j} \right] + G - \rho \varepsilon \quad (3)$$

$$\frac{\partial (\rho \varepsilon)}{\partial t} + \frac{\partial (\rho u_i \varepsilon)}{\partial x_i} = \frac{\partial}{\partial x_j} \left[\left(\mu + \frac{\mu_t}{\sigma_\varepsilon} \right) \frac{\partial \varepsilon}{\partial x_j} \right] + C_{1\varepsilon} \frac{\varepsilon}{k} G - C_{2\varepsilon} \rho \frac{\varepsilon^2}{k} \quad (4)$$

Where ρ is the flow density; μ is the viscosity coefficient; P is the fixed pressure; μ_t is the turbulence viscosity coefficient; G is the turbulent kinetic energy; σ_k is the turbulent prandtl number of k ; σ_ε is the turbulent prandtl number of ε ; generally take $\sigma_k=1.0$, $\sigma_\varepsilon=1.3$, $C_{1\varepsilon}=1.44$, $C_{2\varepsilon}=1.92$; g is the gravity acceleration.

2.2 Geometric Model

Yang *et al.* (2009) obtained through simulation that the axial velocity of the jet was the maximum when the contraction angle was between 12°-16°. The results acquired by predecessors from the aspects of turbulence dissipation rate, nozzle exit section contraction and core zone length show that the jet pump with nozzle aspect ratio range of 0.25-1.00 has better performance (Tan *et al.* 2019). The appropriate throat mouth length range was 1.0-1.7 times of the nozzle diameter proposed by Ge *et al.* (2012). For a better observation on the vapor flow in the throat and diffuser, the throat and the diffuser are lengthened appropriately. In order to keep the fluid steady, 10 mm straight pipe sections are reserved at the inlet and outlet of the jet device. The pipette length is shortened befittingly. Based on the common pipe diameter of 30 mm in the market, the nozzle diameter d_1 is determined to be 3 mm, the throat nozzle distance L_g to be 6 mm, and the diffuser length L_c to be 158 mm ultimately. The total length of the model is $L_d+L_h+L_g+L_k+L_c+L_0=357$ mm. The specific size of each structure is listed in Table 1.

Table 1 Structural parameters of the cavitation jet device

Parameter name	Symbol	Dimension
Inlet diameter	d_i	30.0 mm
Jet nozzle diameter	d_1	3.0 mm
Throat diameter	d_2	5.0 mm
Outlet diameter	d_o	30.0 mm
Suction import diameter	d_0	4.0 mm
Inlet length	L_d	10.0 mm
Contraction length	L_h	133.0 mm
Outlet length	L_0	10.0 mm
Diffuser length	L_c	158.0 mm
Throat length	L_k	40.0 mm
Throat mouth length	L_g	6.0 mm
Converging angle	α	11.9°
Diffusing angle	β	9.0°

Figure 3 illustrates the mesh geometric model of cavitation jet established by GAMBIT and observation region label. It is necessary to extract the internal data of jet device to investigate the flow characteristics. As shown in Fig. 3, the monitoring regions are placed at Plane Z=0 mm and Plane X=146 mm. At Plane Z=0 mm, four longitudinal monitoring lines are set along the X direction and five horizontal monitoring lines are set along the Y direction. X represents the axial distance from the jet inlet. X=169 mm is located in the central throat and X=189 mm is located in the end of throat. X=199 mm and X=209 mm are set in the diffuser. Y=-6 mm, Y=-4 mm, Y=0 mm, Y=4 mm, and Y=6 mm are set successively. Four monitoring points X_p=146 mm (suction chamber), X_p=169 mm (central throat), X_p=199 mm (diffuser chamber) and X_p=209 mm (diffuser chamber) are arranged at the X-axis. The intersection point between the X-axis and the front end of the interface is considered as the initial mutation point. At Plane X=146 mm, the lowest point of boundary between the suction chamber and the pipette is set as the monitoring point of suction port. Hypermesh is the key of ANSYS FLUENT that decides the simulation calculation accuracy. Grid types are Tet/Hybrid and Hex/Wedge respectively. The flow field is complicated due to the mixture of working fluid and absorbed fluid in the suction chamber and the suction port (Lu 2004). The cavitation is prone to alter the single phase distribution in the jet, especially in the transition region between vapor and liquid. Therefore, the suction chamber, suction port and diffuser chamber are critical area to investigate the internal jet fluid movement and the stable suction mechanism with a peculiar mesh refinement. The geometric model grid is adjusted modestly by jet velocity gradient and the mesh quantity amounts to 949291.

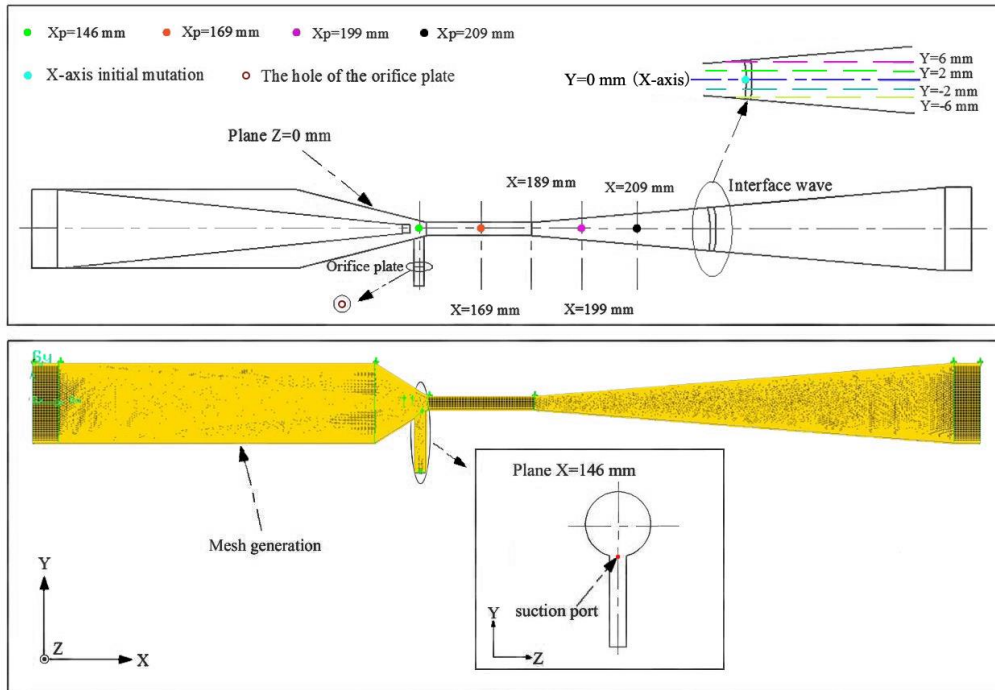


Fig. 3. The GAMBIT model and observation region label.

A mixture model and SIMPLE pressure-velocity coupling mode are adopted referred previous study (Xiao and Long 2015). Simultaneously, the working fluid and the absorbed fluid inlet are set as mass flow inlet, and the fluid outlet is set as the pressure outlet. The fluid boundaries are defined distinctively to make the GAMBIT model closer to reality and the subsequent simulation calculation more accurate by referring to the previous study. The working fluid inlet is set as the mass flow inlet. The absorbed fluid inlet is set as the pressure inlet. The mixed fluid outlet is set as the pressure outlet. The nozzle outlet, throat inlet and throat outlet are set as the interior; other boundaries are set as wall. The mixed phase media is water-liquid and water-vapor with an energy exchange option open. The absorbed liquid media is water-liquid. The vapor phase generated during cavitation is water-vapor, and the dissolved gas in water is negligible. The mixture, transient and $k-\epsilon$ turbulence models are selected in ANSYS FLUENT for simulation. The water-liquid is set to the first phase and water-vapor to the second. The phase interaction is cavitation. The SIMPLE semi-implicit connection pressure equation method is employed to conduct the pressure-velocity coupling. The real-time absorption amount is monitored and saved during the calculation process. When observing the basic characteristics of mutation interface and simulating different pressure ratios, 0.001 s for each step and 50 steps for a total of 0.05 s are set. The mass flow rate is 0.3 kg/s and the inlet pressure is 600 kPa. The suction pressure is atmospheric pressure. The different pressure ratios are set to evaluate the vapor evolution law and absorption amount law of cavitation jet. The hydraulic diameter of inlet/outlet is set as 30 mm and the suction inlet as 4 mm. The turbulence intensity is set as 5%.

2.3 Grid Independence Test

Grid is the minimum computing unit of ANSYS FLUENT. The grid division is directly related to the accuracy of calculation results. In theory, the more accurate the calculation results are when the grid is finely divided. A series of high-quality grid structure models built by Gambit are shown in Fig. 4.

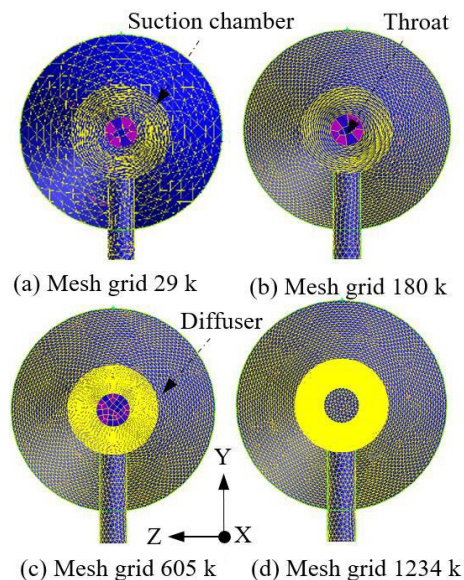


Fig. 4. Meshes of different densities.

We compared absorption amount change with time in Fig. 5 and X-axis pressure in Fig. 6 under different density grids. Seen from Fig. 5, in the case of 29 k and 180 k grids, the corresponding absorption

amount is 0.136 kg/s with error rate of 9.3% and 0.142 kg/s with error rate of 5.3% based on the mesh grid 1234 k, severally. The final absorption amount is around 0.150 kg/s when the grid number over 605 k. The error rate is just 0.6% at the mesh grid 950 k. Similarly, the pressure at the suction port and throat inlet is more consistent and stable when the grid number is greater than 605 k in Fig. 6. The comparison of numerical results shows that with the grid gradual refinement, the data tends to be stable after the grid number reaches 605 k, which proves that the grid mesh over 605 k is fine enough to meet the accuracy requirement of this simulation.

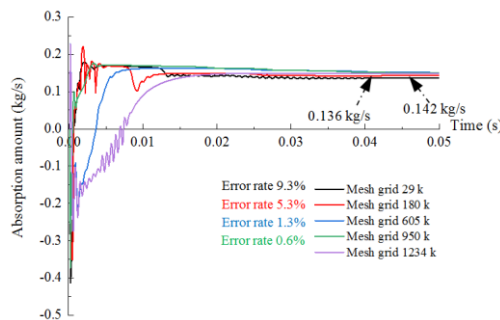


Fig. 5. Absorption amount of different densities.

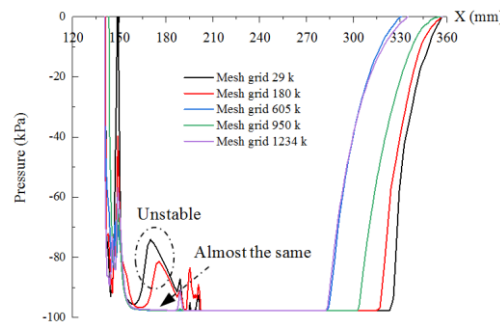


Fig. 6. The X-axis pressure different densities.

3. RESULTS AND DISCUSSIONS

3.1 Vapor Evolution Process in The Cavitation Jet

A significant pressure drop in the contraction tube results in a vapor formation that marks the beginning of cavitation (Payri *et al.* 2013). Figure 7 illustrates the vapor region evolution process at the outlet pressure 0 kPa. The vapor volume fraction at Plane Z=0 mm and Plane X=146 mm is exhibited by the color depth. The red means the pure vapor and the blue means the pure liquid.

It can be seen that vapors first appear in the upper suction chamber and suction port when $t=0.002$ s, and then disappear in the suction port at $t=0.005$ s. Meanwhile, vapors appear in the front and end of the throat. This discovery on the order and location of vapors appearance is similar to the previous literature research with no suction process involved (Lu and Shang 1987; Wu *et al.* 2005). At this point, most of

the vapor volume fraction is 30%-50%. As the time initiates a slight increase, the vapor region and volume fraction both correspond to a sharp grow. The vapors advance from both ends of throat to the center and the diffuser chamber. The suction chamber is full of vapors with the vapor volume fraction of higher than 90% at $t=0.01$ s. Finally, a large region of highly cavitation mixture fluid is formed in the jet device at $t=0.05$ s. During the formation of high-speed jet, the fluid undergo a phase transition when the negative pressure is reduced to the vaporization pressure.

Figure 8 presents the development law of X-axis vapor volume fraction that verifies the generation process of vapors. The vapors initially appear at the suction port with the maximum vapor volume fraction of only 2%, as shown in Fig. 8 (a). As the cavitation develops, the vapors emerge at the front and end of throat that is consistent with the previous cloud diagram. Later, the central throat begins to vaporize, which has risen to 6% at $t=0.01$ s. Then, the vapors invade toward the throat, suction chamber and diffuser. Seen from Fig. 8 (f), the maximum vapor volume fraction can reach about 95% at last that means the cavitation evolution process has fundamentally completed.

In the meantime, the vapor volume fraction on four lines (X=169 mm, X=189 mm, X=199 mm and X=209 mm) and the corresponding vapor distribution cloud diagram are extracted, as shown in Fig 9. The vapor volume fraction decreases from 78% at the boundary to 62% at the interior in the central diffuser (X=209 mm), while it drops sharply from 74% to 0 in the throat (X=169 mm). The previous literatures have indicated that the vaporization is first produced in the circle jet boundary and then the mainstream region at the cavitation condition (Bonnington 1972; Kudirka and Decoster 1979; Marini *et al.* 1992), while this viewpoint is also suitable for the suction process of cavitation jet, which resulting in a higher vapor volume fraction at the boundary than the interior. The vapor distribution shows a little dissymmetry enslaved to the suction port position set in the lower area. As a result, the vapor volume fraction of the negative Y-axis is higher than that of the positive Y-axis, and the lowest vapor volume fraction point lies in the positive Y-axis.

3.2 Mutation Interface

The pressure and vapor region distribution in the jet device at different times are displayed in Fig. 10. It can be found that a narrow vapor and liquid transition section is shaped in the jet that is called mutation interface, where the upstream is vapor region and the downstream is liquid region. During the formation of mutation interface, the front-end diffuser pressure first drops to the vaporization pressure and the vapor volume fraction reaches about 30% at $t=0.005$ s. The vapors then invade into the diffuser and the vapor volume fraction reach up to higher than 90% with the corresponding pressure close to the vaporization pressure. The two phase interface was also proved indirectly by relevant scholars (Brennen 2005; Witte 1969), while there is no suction process mentioned.

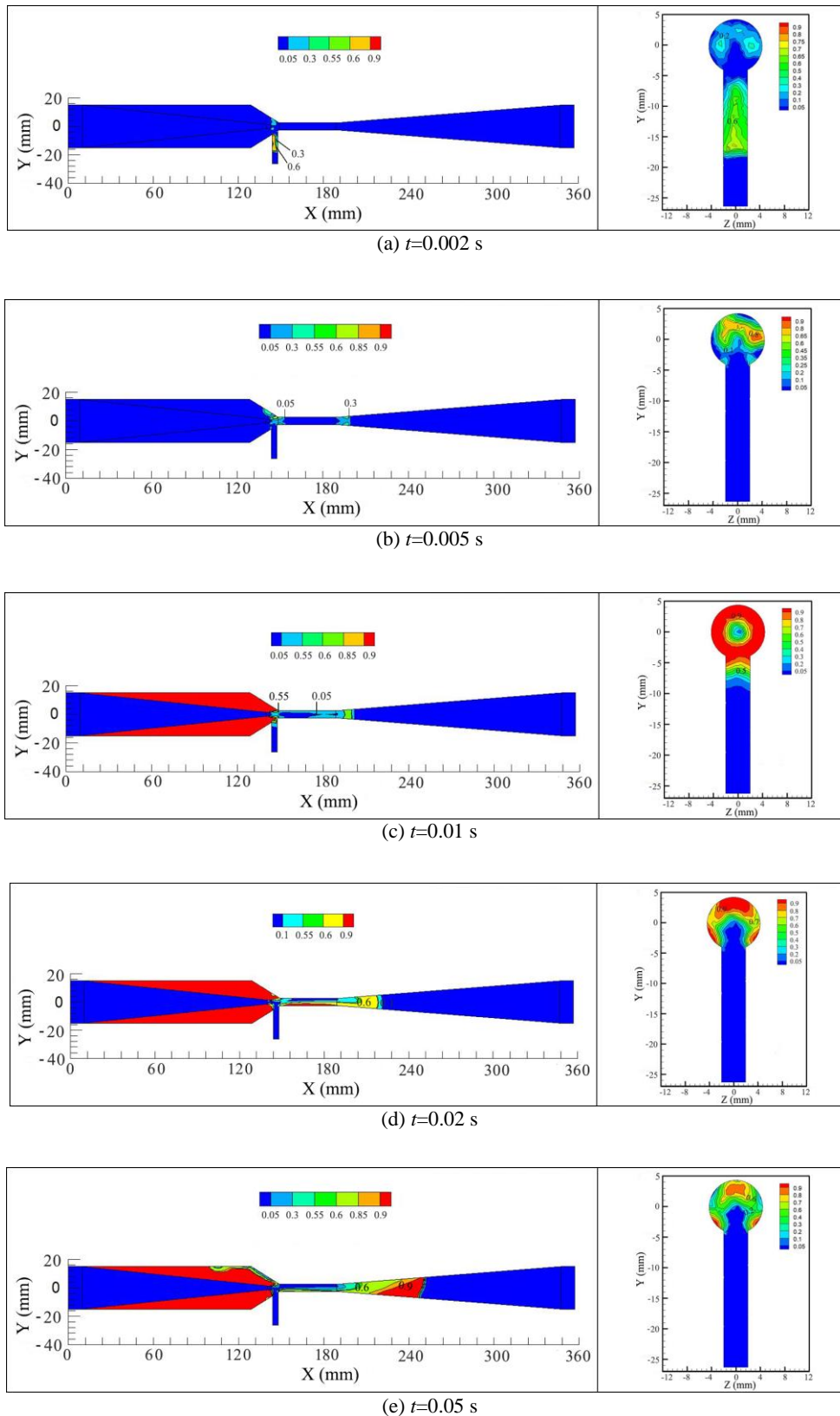


Fig. 7. Vapor region evolution process in the cavitation jet at the outlet pressure of 0 kPa.

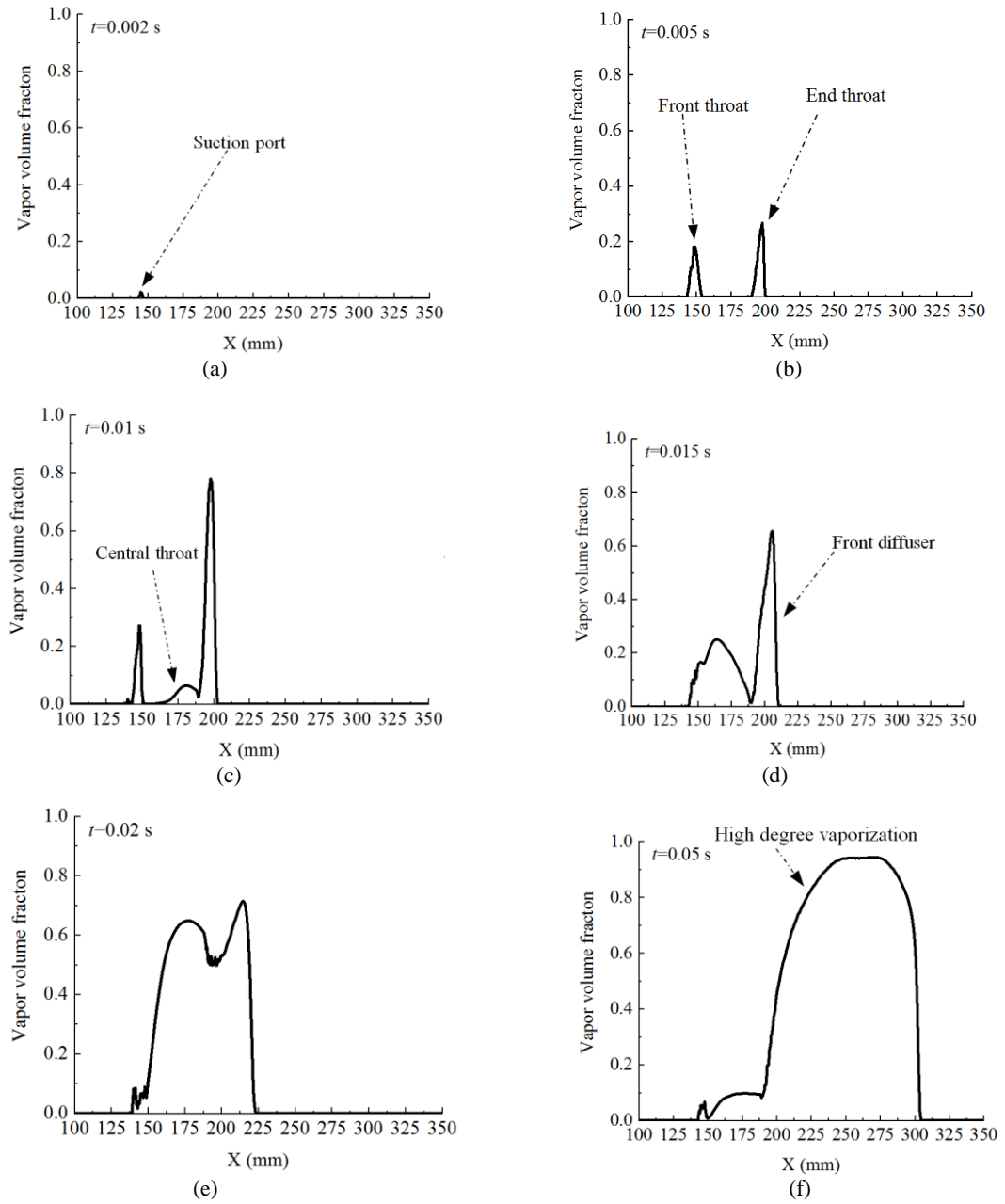


Fig. 8. Development law of X-axis vapor volume fraction.

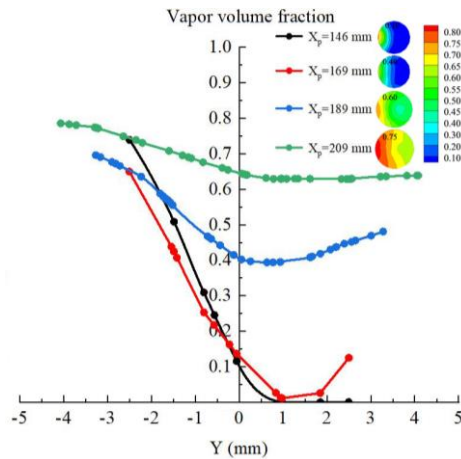


Fig. 9. Vapor volume fraction in the Y direction.

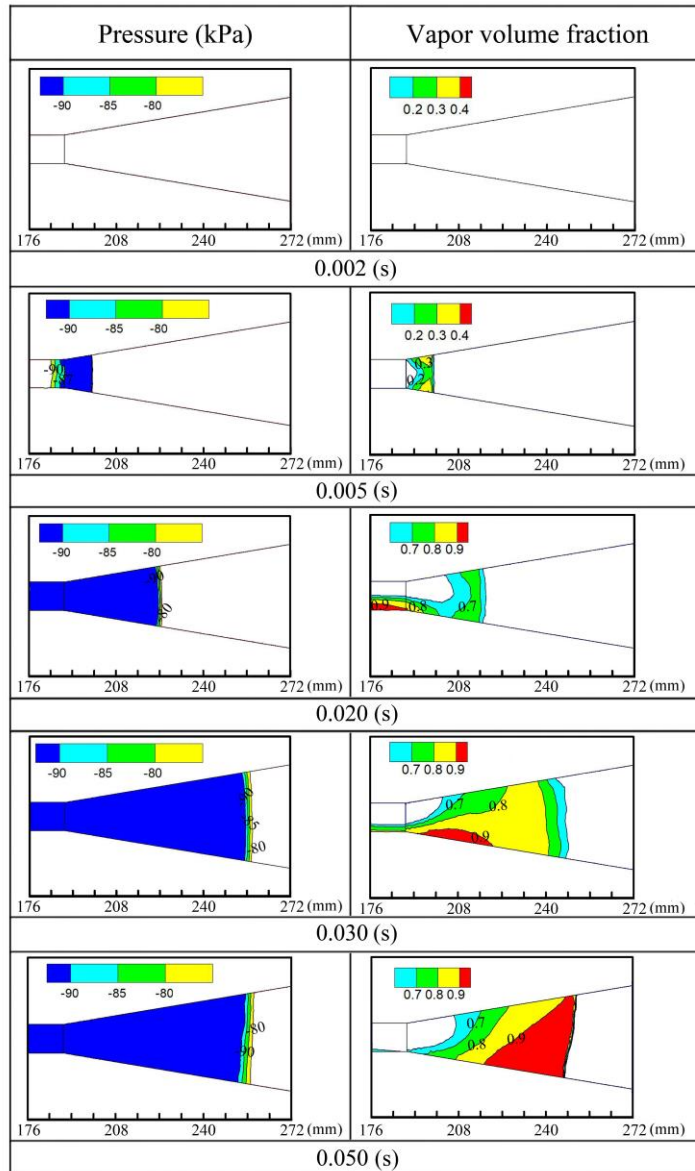


Fig. 10. Mutation interface formation process in the cavitation jet.

Seen from the cloud diagram, the pressure and the vapor volume fraction are clearly stratified at about $X=248$ mm.

The ratio of the outlet pressure to inlet pressure is defined as pressure ratio h . Figure 11 illustrates the X-axis fluid pressure and velocity at $t=0.05$ s under different pressure ratios. When the working fluid flows through the contraction, the velocity increases gradually and the pressure decreases due to the gradual reduction of the flow cross section. A maximum speed of 46 m/s and a minimum pressure of -98 kPa are produced at the nozzle outlet. Subsequently, the working fluid and the absorbed fluid enter the throat together, and the velocity gradually decreases. The pressure is constant at about -98 kPa which is close to the vaporization pressure. Subjected to the upstream vapor and the downstream liquid of interface, the fluid pressure

and velocity exerts a remarkable mutation along the X direction, as indicated by the arrow in Fig. 11. The mutation position is $X=248$ mm at the pressure ratio $h=0$. When X increases from 248 mm to 270 mm, the fluid pressure increases from -98 kPa to -40 kPa with a significant increasing amplitude of 59.2% and the velocity decreases from 27 m/s to 15 m/s with a decreasing amplitude of 44.4%. The mutation law is also confirmed by the pressure ratio $h=0.083$ and 0.292. The mutation exists at $X=206$ mm at the pressure ratio $h=0.292$. When $X=206-209$ mm, the fluid pressure increases from -98 kPa to 0 kPa and the velocity decreases from 27 m/s to 13 m/s with a decreasing amplitude of 51.9%.

From above analysis, it can draw a conclusion that the flow parameters are bound to experience a mutation across the transition interface in the cavitation jet. This is also verified by the mixture

fluid density change. Figure 12 displays the mixture density distributions of mutation interface along five horizontal lines at Plane Z=0. As a whole, the X-axis density ρ^* increases from the lowest 18-76 kg/m³ to 998 kg/m³. On Y=-6 mm, the density ρ^* increases rapidly from the minimum of 18 kg/m³ at X=245 mm to 998 kg/m³ at X=251 mm. On Y=6 mm, the density ρ^* increases from the minimum of 76 kg/m³ at X=250 mm to 998 kg/m³ at X=255 mm. The initial mutation density increases linearly as Y rises. A discovery is obtained by contrast that the closer the jet device is to the bottom, the lower the mixture fluid density is. As Y rises, the mutation interface moves from X=245-251 mm to X=250-255 mm. It can be estimated that the average thickness of mutation interface is 5-6 mm. At both ends of mutation interface boundary, there is a slow density increase region with a width of about 1 mm in the front and 2-3 mm in the back that is called the fuzzy mutation region, as marked in Fig. 12.

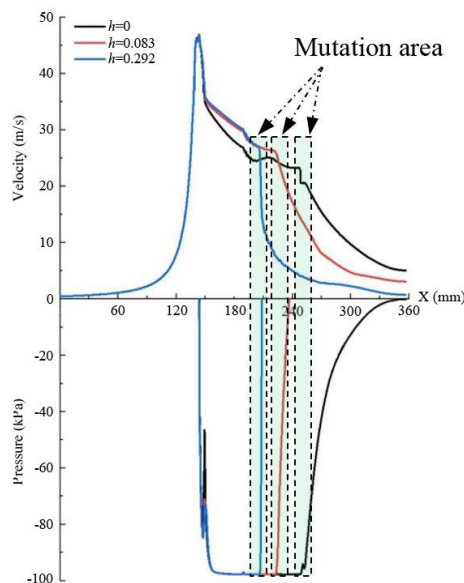


Fig. 11. The X-axis fluid pressure and velocity distribution.

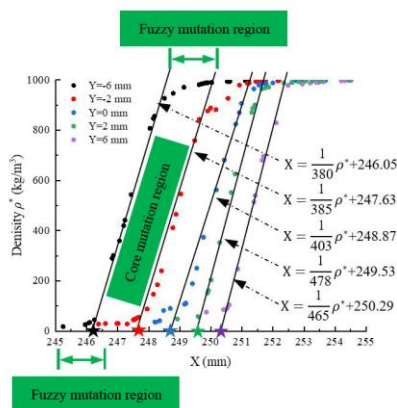


Fig. 12. Mixture density change around the mutation interface.

A sharp density change is present in the central section that is called the core mutation region. A series of fitting curves for ρ^* vs X are drawn in the core mutation region and the corresponding formulas are obtained, as presented in Eq. (5). The density gradient $\frac{\Delta\rho^*}{\Delta X}$ is in the range of 380×10^{-9} - 480×10^{-9} kg/mm⁴. The X-axis intercepts of fitting lines move towards the positive X-axis with the increase of Y.

$$X = \begin{cases} \frac{1}{380 \times 10^{-9}} \rho^* + 246.05 & Y = -6 \text{ mm} \\ \frac{1}{385 \times 10^{-9}} \rho^* + 247.63 & Y = -2 \text{ mm} \\ \frac{1}{403 \times 10^{-9}} \rho^* + 248.87 & Y = 0 \text{ mm} \\ \frac{1}{478 \times 10^{-9}} \rho^* + 249.53 & Y = 2 \text{ mm} \\ \frac{1}{465 \times 10^{-9}} \rho^* + 250.29 & Y = 6 \text{ mm} \end{cases} \quad (5)$$

3.3 Cavitation Vapor Region Influenced by Pressure Ratio

Through changing the operating conditions, the vapor region and vapor volume fraction in the cavitation jet are obtained at various pressure ratio h . Figure 13 displays the vapor region and volume fraction at different pressure ratios on the running time for 0.05 s. The contour distribution lies in the suction section and the vapor volume fraction is along X-axis. It can be seen that the vapor region in the diffuser decreases obviously with the pressure ratio h increasing. The pressure ratio h is 0.308 when the vapors vanish from the diffuser chamber. The corresponding pressure ratio h of vapor disappearance is about 0.500 for the throat and suction chamber. When the pressure ratio h is less than 0.500, vapors mainly distributes in the upper and lower side of suction port, and the maximum volume fraction reaches up to above 90%. Once the pressure ratio h is larger than 0.500, the vapors at the suction port decrease sharply, and the maximum vapor volume fraction drops to only 50%-60%. The maximum X-axis vapor volume fraction decreases from 96.4% to 0. As a sign, the mutation area moves toward the upstream until vanishes in the suction chamber. The vapor volume fraction decline in the suction port means the vaporization environment is being broken down.

The changes of vapor volume fraction at four points along X-axis ($X_p=146$ mm, $X_p=169$ mm, $X_p=199$ mm and $X_p=209$ mm) are recorded under different pressure ratios, as shown in Fig. 14. The critical pressure ratio that keeps the vapor volume fraction no longer to be constant is defined as h^* . The critical pressure ratio that the vapor volume fraction declines to 0 is defined as h^{**} . At point $X_p=209$ mm (in the diffuser), the vapor volume fraction is unable to keep stable at the pressure ratio $h^*=0.275$ and decreases to 0 at the pressure ratio $h^{**}=0.308$. The critical pressure ratio h^* and the critical pressure ratio h^{**} are 0.325 and 0.417 at point $X_p=169$ mm (central throat). While, the critical pressure ratio h^* and the critical pressure ratio h^{**} at point $X_p=146$ mm (suction port)

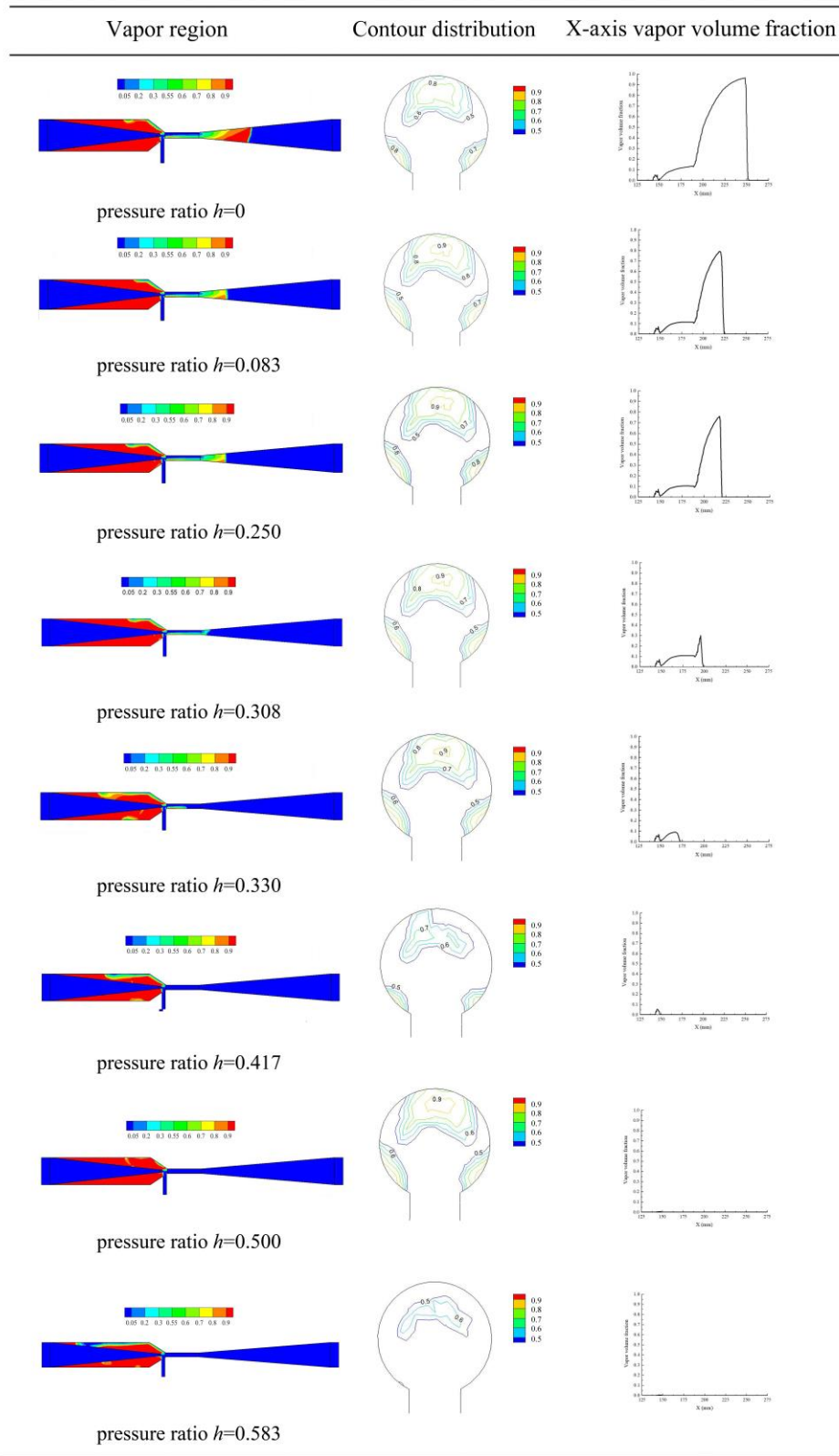


Fig. 13. Vapor region and volume fraction at different pressure ratios.

are 0.417 and 0.500, respectively. It can be concluded that the closer the point is to the jet inlet, the larger the critical pressure ratio h^* and the critical pressure ratio h^{**} are. The main reason is that the

vaporization region is gradually pushed from the outlet to the inlet with the increase of the pressure ratio h , which is also consistent with the trend present in Fig. 13. As the mutation interface migrates toward

the upstream region, the previous upstream vaporization environment is changed. Once the mutation interface moves to the suction chamber, the vaporization environment in the suction port is destroyed and absorption process will be affected.

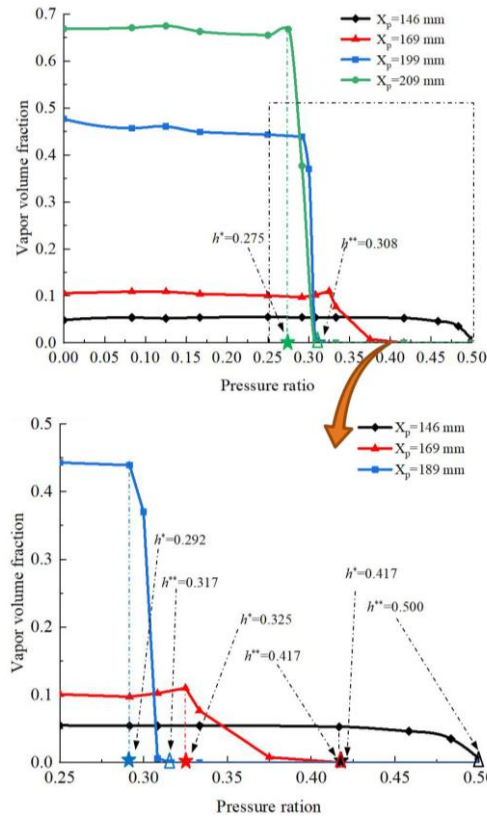


Fig. 14. Vapor volume fraction at different positions of X-axis.

The critical pressure ratio that causes significant changes in negative pressure and initial mutation density is defined as h_0 . Figure 15 illustrates the relationship between the X-axis initial mutation density and negative pressure at suction port. The initial density varies from 36 to 998 kg/m³ and the negative pressure p_0 keeps in constant at about -89(-87) kPa when the pressure ratio lies in the range of 0-0.5. Once the critical pressure ratio h_0 is crossed, the initial mutation density climbs to the liquid water density at 998 kg/m³ and the stable negative pressure condition is destroyed. There are two reasons responsible for this phenomenon. For one hand, the mutation interface exists when the pressure ratio h is less than the critical pressure ratio h_0 , which ensures the stability of negative pressure (Lu *et al.* 2015). The formation of vapor is closely related to the pressure ratio h (Abdulaziz 2014) and the evaporation degree becomes weakened with raising the pressure ratio. As a result, the capacity of mutation interface to resist the downstream fluctuation decreases with the reduction of vapor volume fraction. For the other hand, the pressure ratio has a great influence on the pressure distribution in the jet device (Long *et al.* 2008). The disappearance of mutation interface results in the

absence of negative pressure to maintain stability when h_0 is surpassed. Therefore, it can be predicted that the precise quantitative control is achievable before the disappearance of mutation interface.

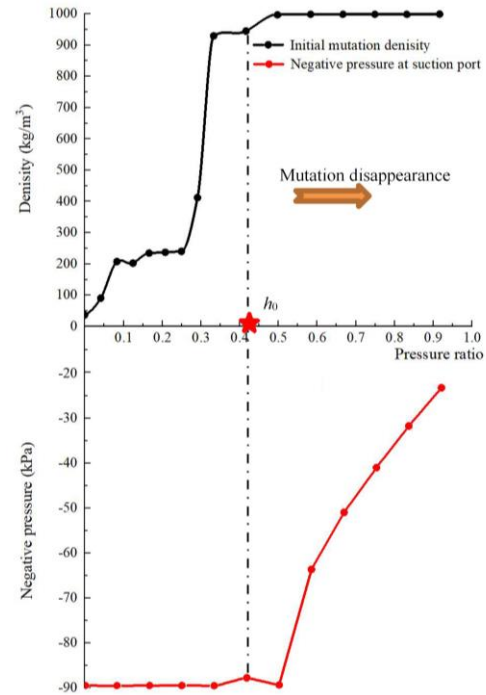


Fig. 15. Initial density and negative pressure under different pressure ratios.

3.4 Agent Precise Quantitative Control

The suction performance of cavitation jet is depended on the pressure difference between the suction port and external environment. A stable negative pressure in the suction port is destined to create a good environment for suction. Figure 16 illustrates the relationship between the negative pressure p_0 and absorption amount q that are monitored at 0.05 s.

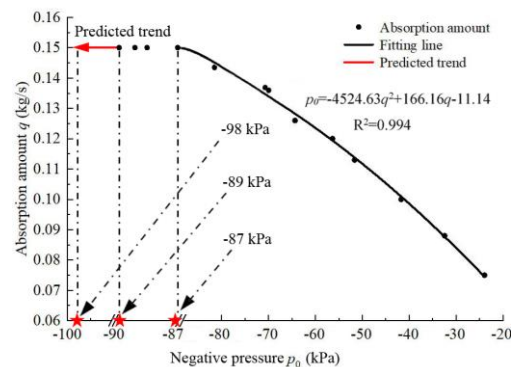


Fig. 16. Relationship between the negative pressure and absorption amount.

With the continuous decrease of negative pressure p_0 , the absorption amount q presents a regular rise. It is obvious that the growth rate of absorption amount

q decreases gradually with the decrease of negative pressure p_0 . Thus, a fitting curve of q vs p_0 is drawn based on the quadratic function, as shown in Eq. (6).

$$p_0 = -4524.63q^2 + 166.16q - 11.14 \quad (6)$$

It is also found that the absorption amount q always maintains at 0.150 kg/s and the growth rate reduces to 0 when the negative pressure p_0 is -89(-87) kPa. Thus, the precise quantitative control has been achieved since $p_0 < -87$ kPa. Meanwhile, it can be predicted that the absorption amount q can still remain at 0.150 kg/s when p_0 drops to less than -89 kPa.

The fluid viscosity may produce frictional resistance and then exert an effect on the stable absorption amount when the foaming agent is sucked (Li 2012; Stupa and Chernyshov 1990). Hence, the stable suction capacity of cavitation jet and the data accuracy are tested by changing the absorbed liquid viscosity at different mesh densities, as shown in Fig. 17.

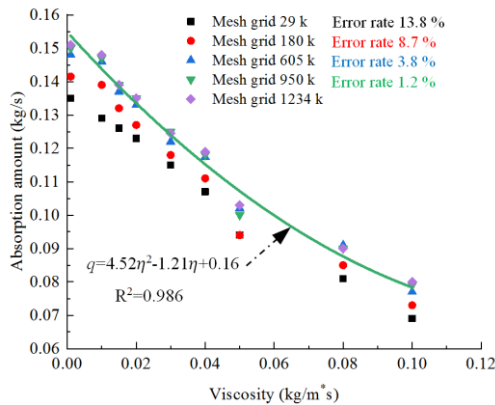


Fig. 17. Relation between the injection liquid viscosity and absorption amount.

As the agent viscosity increases, the absorption amount q decreases gradually along with a decline in the reduction rate at different mesh grids. Based on mesh grid 1234 k, the error rates are obtained under different mesh densities with viscosity of 0.10 kg/m³·s. The simulation accuracy in this paper is demonstrated by the error rate of only 1.2% at the mesh grid of 950 k. When the high-viscosity agent is rubbing with the pipe surface, the frictional resistance and energy consumption rises, which leads to the reduction of absorption amount under the same operation conditions. The fitting curve of q vs η is shown in Eq. (7) with mesh grid of 950 k.

$$q = 4.52\eta^2 - 1.21\eta + 0.16 \quad (7)$$

For the purpose of evaluating the quantitative control performance and the mesh accuracy at different levels, a series of resistance test is conducted in the suction pipe that is reflected by the orifice plate set in the center pipette. Seven-level hole sizes of orifice plate are employed. The specific diameter and hole area are listed in Table 2.

Table 2 Hole area of the orifice plate

Jet pump ID	Hole radius (mm)	Hole area (mm ²)
A	0.798	2.00
B	1.128	4.00
C	1.382	6.00
D	1.596	8.00
E	1.784	10.00
F	1.913	11.50
G	2.000	12.57

Figure 18 presents the real-time change of absorption amount q at different orifice plate hole areas s with mesh grid 950 k. The absorption amount q experiences a transient fluctuation at the initial stage, while it is clear that each cavitation jet realizes a constant absorption amount eventually. The constant absorption amount q rises with the orifice plate hole area s increasing, and the rate of growth is increasing.

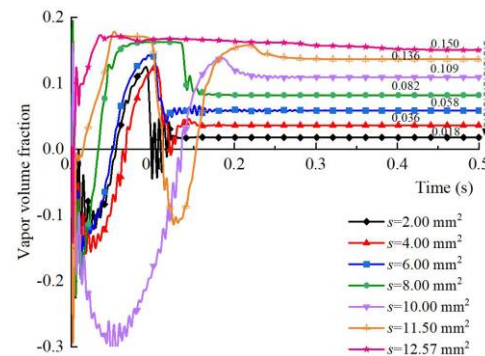


Fig. 18. Real-time change of absorption amount at different orifice hole areas.

The absorption amount q is 0.150 kg/s at $s = 12.57$ mm², while it has decreased sharply to 0.018 kg/s at $s = 2.00$ mm² when the mesh grid is 950 k. The curvilinear relationship between the absorption amount q and hole area s is shown in Fig. 19. The error rate is compared under different mesh densities when $s = 12.57$ mm² based on mesh grid 1234 k. The error rate is only 2.0% when the number of grids reaches 605 k, indicating that the current grid density is sufficient to meet the requirements.

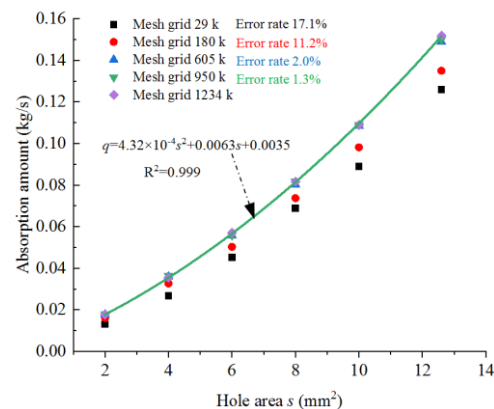


Fig. 19. Relation between the hole area and absorption amount.

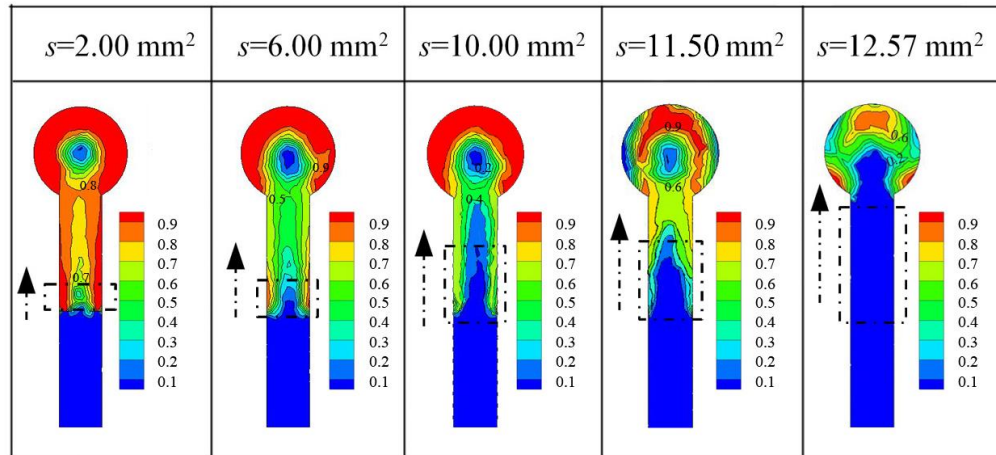


Fig. 20. Vapor volume fraction at different orifice plate hole areas.

Correspondingly, Fig. 20 shows the vapor distribution cloud diagram of Plane X=146 mm under five different orifice plate hole areas s ($s=2.00 \text{ mm}^2$, $s=6.00 \text{ mm}^2$, $s=10.00 \text{ mm}^2$, $s=11.50 \text{ mm}^2$ and $s=12.57 \text{ mm}^2$) with mesh grid 950 k. It can be seen that there are masses of vapors in the suction chamber and pipette, which is the premise for the stable suction of cavitation jet. The space above the orifice plate is occupied by vapors when the orifice plate hole areas s is small, which blocks the further increase of the absorption amount q . With the gradual enlargement of orifice plate hole area s , the vapor region and vapor volume fraction in the pipette gradually decrease. Simultaneously, the absorbed liquid passing through the orifice plate gradually increases, which is consistent with the gradual increase of the absorption amount q in Fig. 20. The orifice plate changes the fluid velocity distribution that induces some whirlpool in the pipette, which causes the local loss (Razinov and Steepochkin 2001). The smaller the orifice plate hole area s is, the greater the local loss is, and then the smaller the absorption amount q is. The research result of the orifice plate hole test has a guiding significance for the agent precious control when the control valve is set in the suction pipe to obtain a various quantitative control level. Although the paper research content is conducted based on a fixed jet structure size, it is believed that the core dates obtained in this paper will provide a key reference for the further design of the cavitation jet that achieves optimum performance.

4. EFFECT ANALYSIS IN THE PRACTICAL

As a coal transport terminal, the coal bunker is the main dust source for most thermal power station (Yang and Ma 2016). The coal bunker dust is mainly caused by the masses of crushed coal fall from the high coal chute, which can reach as high as 1000 mg/m^3 in the local region of coal bunker. This dust prevention becomes difficult due to its suspension and hydrophobic properties (Zhang *et al.* 2019). The water spraying was widely used previously to control

the coal bunker dust, while it was proved to be undesirable subjected to its poor dust control efficiency, especially for the small-size particle dust. Whose still, water spraying was only effective for a short-time period and the dust control effect was easy to be influenced by the drop size, velocity, distribution, spray condition (Xi *et al.* 2017). As for other dust control methods, like magnetization dust depression, need specially designed and costly generators and complex devices that restrict the technical applicability (Nie *et al.* 2016). Therefore, it starves for a new dust control measure using adhesive foam to deal with the technical problem.

To evaluate the effectiveness of the proposed precise control method using the cavitation jet, a series of performance test is conducted in a foam technology used for dust suppression in a cylindrical coal bunker. The manufacture physical dimension of the cavitation jet refers to Table 1. The mass flow rate is maintained at about $1.0\text{-}1.2 \text{ m}^3/\text{h}$ at working pressure 600 kPa. As shown in Figure 21, two pressure gage, P_1 , P_2 , are set in the water pipeline to monitor the inlet pressure and outlet pressure. The negative pressure meter P_s is set in the suction pipeline to monitor the suction pressure. A foam maker is used to generate the expansion foam that is layed behind the cavitation jet device. Through testing the transmission pressure caused by the foam flow, a critical outlet pressure of cavitation jet is defined and then the operation condition is determined. The critical outlet pressure is set in the range of $0.2\text{-}0.3 \text{ MPa}$ to meet the minimum requirements of foam transmission and terminal spray. For the purpose of agent backflow into the vessel, the gas pressure is controlled at 180 kPa that is less than the critical pressure. As the vaporization condition is created, a constant negative pressure is produced, which is constant at -94 kPa , and a stable absorption amount of 0.018 kg/s is achieved as expected with a fluctuation error less than 3%. The actual precision of agent absorption amount is less than 6% on the cavitation condition. Without any additional control units, the successful achievement on the precise agent addition ensures the reliable foam production and simplifies the system operation significantly.

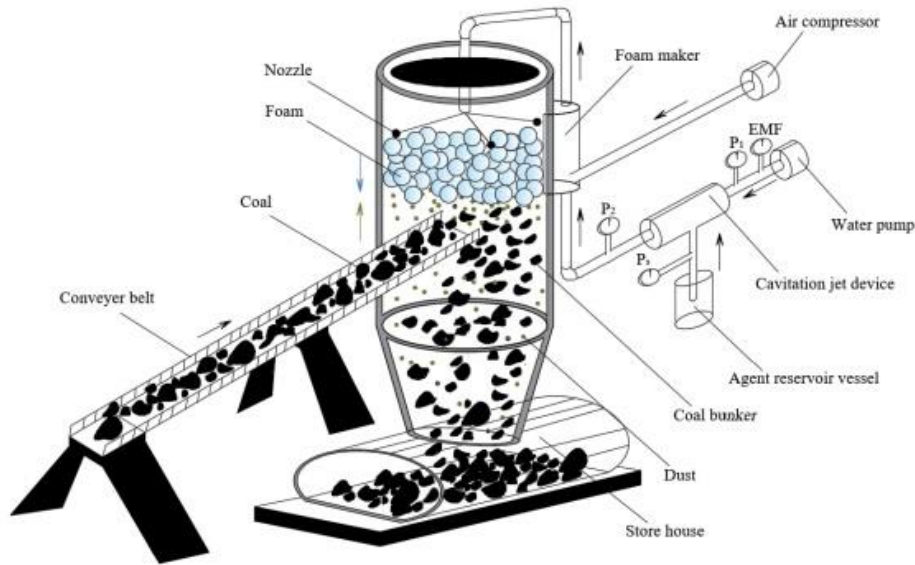


Fig. 21. Field practical of cavitation jet device in the coal bunker.

Figure 21 illustrates the dust production process in the cylindrical coal bunker. Coals transferred by the conveyer belt fall into the coal bunker bottom at the belt tail. The falling dust particles produce massive float dust, which move upwards due to buoyancy. Since the coal bunker roof is the main dust produce area (Wang 2017), the foam spraying nozzles are circular layout at the top of coal bunker with the maximum coverage angel 120°. The cavitation jet device and foam maker are both hung in the feed channel outside. The foam maker is arranged at the external upper coal bunker. The foaming agent reservoir vessel is place in the ground and the agent is sucked from a suction hose. The water pump is employed to provide the pressure water and the air compressor is employed to supply gas. When the expansion foams are sprayed from the upper nozzles, they capture, cover, pack and then clear the rising dust particles. Three representative sampling points are set around the coal fall position in the conveyer belt tail, where the dust concentration is relatively high than other region. Through arranging the foaming system and dust sampling points in the coal bunker, the dust suppression effect using adhesive foam is investigated and evaluated.

The test data indicates that the adhesive foam makes the average concentration of total dust drop from 633.2 mg/m³ to 78.6 mg/m³, achieving 87.6% dust suppression efficiency, and the suppression efficiency of respirable dust is 89.2%, which is 2.4 and 2.7 times of conventional water spraying, respectively. More importantly, the foam preparation requires a water consumption rate of 0.5 m³/s that is only 20%-25% of conventional water spraying, which saves the water resource and improves the working environment greatly. From the beginning to end of technology implementation, a stable absorption amount of foaming agent is controlled precisely at 0.0025 m³/h and the agent cost input is

estimated to be rather low. The reliable control system, high dust suppression efficiency and remarkable economic benefit indicate that the proposed agent control method is effectiveness and practical, which provides a key technical support for the widespread application of foam technology used for dust suppression.

5. CONCLUSION

- (1) The vapor appearance order is suction port, suction chamber, throat front and end, diffuser and central throat of the cavitation jet. The maximum vapor volume fraction increases with time until reaches over 90%. A distinct vapor-liquid interface with the thickness 5-6 mm is found between the vapor region and downstream liquid region. In the mutation interface, the X-axis pressure increases by 59.2% and velocity decreases by 44.4%, and the density gradient is 380×10^{-9} - 480×10^{-9} kg/mm⁴.
- (2) The vapor region in the cavitation jet decreases and the maximum X-axis vapor volume fraction declines from 96.4% to 0 with the increase of pressure ratio. The mutation interface moves towards the upstream continuously until disappears. The X-axis initial mutation density increases from 36 kg/m³ to 998 kg/m³ and the negative pressure remains at about -89-(-87) kPa when the pressure ratio is 0-0.500. As the critical pressure ratio crossed, the X-axis initial mutation density keeps unchanged and the stable negative pressure cannot be maintained.
- (3) The absorption amount maintains at 0.150 kg/s when the negative pressure lies in -89-(-87) kPa. While, the relation between absorption

amount and negative pressure is quadratic equation as the negative pressure larger than critical value -87 kPa. As the absorbed liquid viscosity increases, the absorption amount decreases gradually. The cavitation jet can stabilize different quantitative control levels with the orifice plate hole area change. The absorption amount decreases with the reduction of orifice plate hole area.

- (4) The successful dust suppression practical in the coal bunker indicates that the new agent addition method using the cavitation jet is scientificity and effectiveness. The precision of agent absorption amount is controlled at less than 5% and the foam efficiencies on suppressing total dust and respirable dust reach 87.6% and 89.2%. It is foreseeable that the reliable control method is destined to be a highly promising technology in the foam industry and other related field.

ACKNOWLEDGEMENTS

This work was supported by the National Natural Science Foundation of China (52074304; 51704299), Open Research Project of the State Key Laboratory of Coal Resources and Safe Mining (China University of Mining and Technology) (SKLCSRSM17KFA10), Open Research Project of state Key Laboratory Cultivation Base for Gas Geology and Gas Control (Henan Polytechnic University) (WS2018A03), and the Yue Qi Young Scholar Program of China University of Mining and Technology, Beijing.

REFERENCES

- Abdulaziz, A. M. (2014). Performance and image analysis of a cavitating process in a small type venturi. *Experimental Thermal and Fluid Science* 53, 40-48.
- Abedini, A. E., A. Ashrafizade and H. M. Karimi (2014). Experimental performance evaluation of a cavitating venturi. *Arabian Journal for Science and Engineering* 39(2), 1375-1380.
- Aloui, F. and S. Madani (2007). Experimental investigation of a wet foam flow through a horizontal sudden expansion. *Experimental Thermal and Fluid Science* 32(4), 905-926.
- Bonnington, S. T (1972). Jet pumps and ejectors: A state of the art reviews and bibliographer. *BHRA Fluid Engineering* England.
- Brennen, C. E (2005). *Fundamentals of multiphase flows*. Cambridge University Press. Cambridge.
- Cunningham, R. G., A. G. Hansen and T. Y. Na (1970). Jet pump cavitation. *Journal of Fluids Engineering* 92, 483-494.
- Dong, Z. Y (2005). *Jet Mechanics*. Science Press. Beijing.
- Ge, Y. J., Q. Ge and J. Yang (2012). Numerical Simulation and Confirming of Optimal Range on the Nozzle-to-throat Clearance of Liquid-gas Jet Pump. *Fluid Machinery* 40(4), 21-24.
- Ghassemi, H. and H. F. Fasih (2011). Application of small size cavitating venturi as flow controller and flow meter. *Flow Measurement and Instrumentation* 22(5), 406-412.
- Harvey, D. W. (1970). Throttling venturi valves for liquid rocket engines. In: *AIAA joint propulsion conference and exhibit*. Redondo Beach, California, USA.
- Hernandez-Alvarado, F., S. Kleinbart, D. V. Kalaga, S. Banerjee, J. B. Joshi and M. Kawaji (2018). Comparison of void fraction measurements using different techniques in two-phase flow bubble column reactors. *International Journal of Multiphase Flow* 102, 119-129.
- Huzel, D. K. and D. H. Huang (1992). Modern engineering for design of liquid propellant rocket engines. *AIAA*. New York.
- Jia, Z. M., J. T. Mu and Z. L. Fan (1993). *Vortex Pump, Liquid Ring Pump, Jet Pump*. China Machine Press. Beijing.
- Kudirka, A. A. and M. A. Decoster (1979). Jet pump cavitation with ambient and high temperature water. *Journal of Fluids Engineering* 101, 93-99.
- Li, W. G. (2012). Effects of blade exit angle and liquid viscosity on unsteady flow in centrifugal pumps. *Proceedings of the Institution of Mechanical Engineers, Part A: Journal of Power and Energy* 226(4), 580-599.
- Long, X., H. Yao and J. Zhao (2008). Investigation on mechanism of critical cavitating flow in liquid jet pumps under operating limits. *International Journal of Heat and Mass Transfer* 52(9), 2415-2420.
- Lu, H. Q (2004). *Jet Technology Theory and Application*, Wuhan University Press. Wu Han.
- Lu, H. Q. and H. Q. Shang (1987). Mechanism and calculation theory of jet pump cavitation. *Scientia Sinica. Series A* 11(9), 981-992.
- Lu, X. X., D. M. Wang, W. Shen and K. Cao (2014). A new design of double-stage parallel adding equipment used for dust suppression in underground coal mines. *Arabian Journal for Science and Engineering* 39(11), 8319-8330.
- Lu, X. X., D. M. Wang, W. Shen, C. B. Zhu and G. S. Qi (2015). Experimental investigations on liquid absorption of jet pump under operating limits. *Vacuum* 114, 33-40.
- Marini, M., A. Massardo and A. Satta (1992) Low area ratio aircraft fuel jet-pump performance with and without cavitation. *Journal of Fluids Engineering* 114(4), 626-631.
- Morgut, M., E. Nobile and I. Bilus (2011). Comparison of mass transfer models for the numerical prediction of sheet cavitation around a hydrofoil. *International Journal of*

- Multiphase Flow* 37(6), 620-626.
- Nie, W., X. Ma, W. M. Cheng, Y. H. Liu, L. Xin, H. T. Peng and W. L. Wei (2016). A novel spraying/negative-pressure secondary dust suppression device used in fully mechanized mining face: A case study. *Process Safety and Environmental Protection* 103, 126-135.
- Payri, R., F. J. Salvador, J. Gimeno and O. Venegas (2013). Study of cavitation phenomenon using different fuels in a transparent nozzle by hydraulic characterization and visualization. *Experimental Thermal and Fluid Science* 44, 235-244.
- Razinov, Y. I. and B. F. Steepochkin (2001). Pipelines of Complex Configuration. Calculation of the Pressure Loss in Pneumatic Transport with a Stagnated Dense Bed. *Chemistry and Technology of Fuels and Oils* 37(6), 432-435.
- Shah, A., I. R. Chughtai and M. H. Inayat (2011). Experimental and numerical analysis of steam jet pump. *International Journal of Multiphase Flow* 37(10), 1305-1314.
- Shih, T. H., W. W. Liou, A. Shabbir, Z. Yang and J. Zhu (1995). A new $k-\epsilon$ eddy viscosity model for high Reynolds number turbulent flows. *Computers and Fluids* 24(3), 227-238.
- Stupa, V. I. and Y. A. Chernyshov (1990). Dependence of gear-pump operation on viscosity of the metered liquid. *Fibre Chemistry* 21(6):453-455.
- Tan, J., J. M. Zhu and X. P. Long (2019). Numerical analysis of nozzle length-diameter ratio in liquid jet pump. *Water resource and power* 37(9), 151-154.
- Tseng, C. and L. Wang (2014). Investigations of empirical coefficients of cavitation and turbulence model through steady and unsteady turbulent cavitating flows. *Computers and Fluids* 103, 262-274.
- Ulas, A (2005). Passive flow control in liquid-propellant rocket engines with cavitating venturi. *Flow Measurement and Instrumentation* 17(2), 93-97.
- Wang, D. M (2015). *Mine Dusts*. Science Press. Beijing.
- Wang, H. T., D. M. Wang, X. X. Lu, Q. C. Gao, W. X. Ren and Y. K. Zhang (2012). Experimental investigations on the performance of a new design of foaming agent adding device used for dust control in underground coal mines. *Journal of Loss Prevention in the Process* 25(6), 1075-1084.
- Wang, J. B. (2017). Research and application of top type cloth bag cleaner for dust and gas comprehensive control in ground coal bunker. *China Energy Conservation and Environmental Protection* 39(12), 289-292.
- Witte, J. H. (1969). Mixing shock in two-phase flow. *Journal of Fluid Mechanics* 36, 639-655.
- Wu, Y. P., Z. H. Wang and G. Z. Xie (2005). The New progress in research on anti-cavitation materials of hydraulic machinery. *Mechanical Engineering and Materials Science* 29, 5-7.
- Xi, Z. L., S. H. Zhou and L. Z. Jin (2019). Experimental investigation of self-hardening foam-sol for controlling diffusion of static coal dust. *Powder Technology* 345, 274-282.
- Xi, Z. L., Z. Y. Feng and A. Li (2017). Synergistic coal dust control using aqueous solutions of thermoplastic powder and anionic surfactant. *Colloids and Surfaces A* 520, 864-871.
- Xiao, L. Z. and X. P. Long (2015). Influence of inclined angle on cavitation performance of annular jet pump. *Journal of Zhejiang University* 49(1), 123-129.
- Yang, B. B. and R. T. Ma (2016). Power plant coal bunker dust cause analysis. *Huadian Technology* 38(10), 44-46.
- Yang, G. L., X. H. Li, W. H. Zhou and L. Chen (2009). The influence of conical nozzle geometric parameters on the property of efflux flow field. *Chinese Hydraulics and Pneumatics* 5, 62-64.
- Zhang, H. H., W. Nie, J. Y. Yan, Q. Bao, H. K. Wang, H. Jin, H. T. Peng, D. W. Chen, Z. Q. Liu and Q. Liu (2019). Preparation and performance study of a novel polymeric spraying dust suppression agent with enhanced wetting and coagulation properties for coal mine. *Powder Technology* 345, 274-282.
- Zhu, X. L., D. M. Wang, C. H. Xu, Y. F. Zhu, W. D. Zhou and F. He (2018). Structure influence on jet pump operating limits. *Chemical Engineering Science* 192, 143-160.
- Zhu, X. L., D. M. Wang, H. T. Wang, Y. F. Zhu and C. H. Xu (2017). A cavitating device for mini quantitative liquid addition. *Flow Measurement and Instrumentation* 57, 87-93.